The Urban Heat Island of the North-Central Texas Region and Its Relation to the 2011 Severe Texas Drought

A. M. E. WINGUTH AND B. KELP

University of Texas at Arlington, Arlington, Texas

ABSTRACT

Hourly surface temperature differences between Dallas–Fort Worth, Texas, metropolitan and rural sites have been used to calculate the urban heat island from 2001 to 2011. The heat island peaked after sunset and was particularly strong during the drought and heat wave in July 2011, reaching a single-day instantaneous maximum value of 5.4°C and a monthly mean maximum of 3.4°C, as compared with the 2001–11 July average of 2.4°C. This severe drought caused faster warming of rural locations relative to the metropolitan area in the morning as a result of lower soil moisture content, which led to an average negative heat island in July 2011 of −2.3°C at 1100 central standard time. The ground-based assessment of canopy air temperature at screening level has been supported by a remotely sensed surface estimate from the Moderate Resolution Imaging Spectroradiometer (MODIS) on board the *Terra* satellite, highlighting a dual-peak maximum heat island in the major city centers of Dallas and Fort Worth. Both ground-based and remotely sensed spatial analyses of the maximum heat island indicate a northwest shift, the result of southeast winds in July 2011 of ~2 m s^{-1} on average. There was an overall positive trend in the urban heat island of 0.14°C decade^{-1} in the Dallas–Fort Worth metropolitan area from 2001 to 2011, due to rapid urbanization. Superimposed on this trend are significant interannual and decadal variations that influence the urban climate.

1. Introduction

Urban areas are generally warmer than rural locations (Howard 1833), a phenomenon known as the urban heat island effect (UHI; Oke 1973). The urban heat island is commonly estimated by the difference in temperature measurements between stations in urbanized areas and rural areas (e.g., Chandler 1961, 1965; Oke 1973, 1982, 1987). Within this context, rural areas are defined as landscapes that are predominantly natural and not covered with buildings, parking areas, roads, or other man-made urban surfaces (Stewart 2011a). The atmospheric heat island extends vertically through the urban boundary layer, the lower part of which is the urban canopy layer, reaching from ground level to mean building height (Oke 1982; Arnfield 2003). The urban canopy layer UHI is characterized by microscale processes affected by various features of urbanization, like urban canyon geometry and the associated reduction of the sky-view factor [the ratio of the amount of sky "seen" from a given point on a surface; Oke (1978); Stewart (2011a)], increased thermal admittance of urban surfaces, hydrological differences between rural and urban sites (Roth 2007), sensible heat storage of urban surfaces, reduced wind speed and albedo in response to increased surface roughness (Landsberg 1981; Christen and Vogt 2004; Voogt 2010), advective heat contribution from upstream urban areas (Zhang et al. 2011), and other related factors, like anthropogenic heat flux linked to population density with associated building and traffic heat loss (Oke 1987). The climate of the urban boundary layer is determined, at least partially, by the exchanges of momentum, heat, and water with the urban canopy layer.

The maximum canopy layer UHI typically occurs after sunset, especially during periods of low wind speed and clear skies, due to maximum differences between the cooling rates of urban and rural surfaces under these conditions (Runnalls and Oke 2000). Advection can shift the UHI in a downwind direction, a phenomenon first documented by a theoretical analysis (Vukovich 1971) and supported by the Metropolitan Meteorological Experiment (METROMEX) campaign (Wong and Dirks 1978). Strong gradients in temperature, humidity,

Corresponding author address: Arne Winguth, Dept. of Earth and Environmental Sciences, University of Texas at Arlington, 500 Yates St., Arlington, TX 76019.
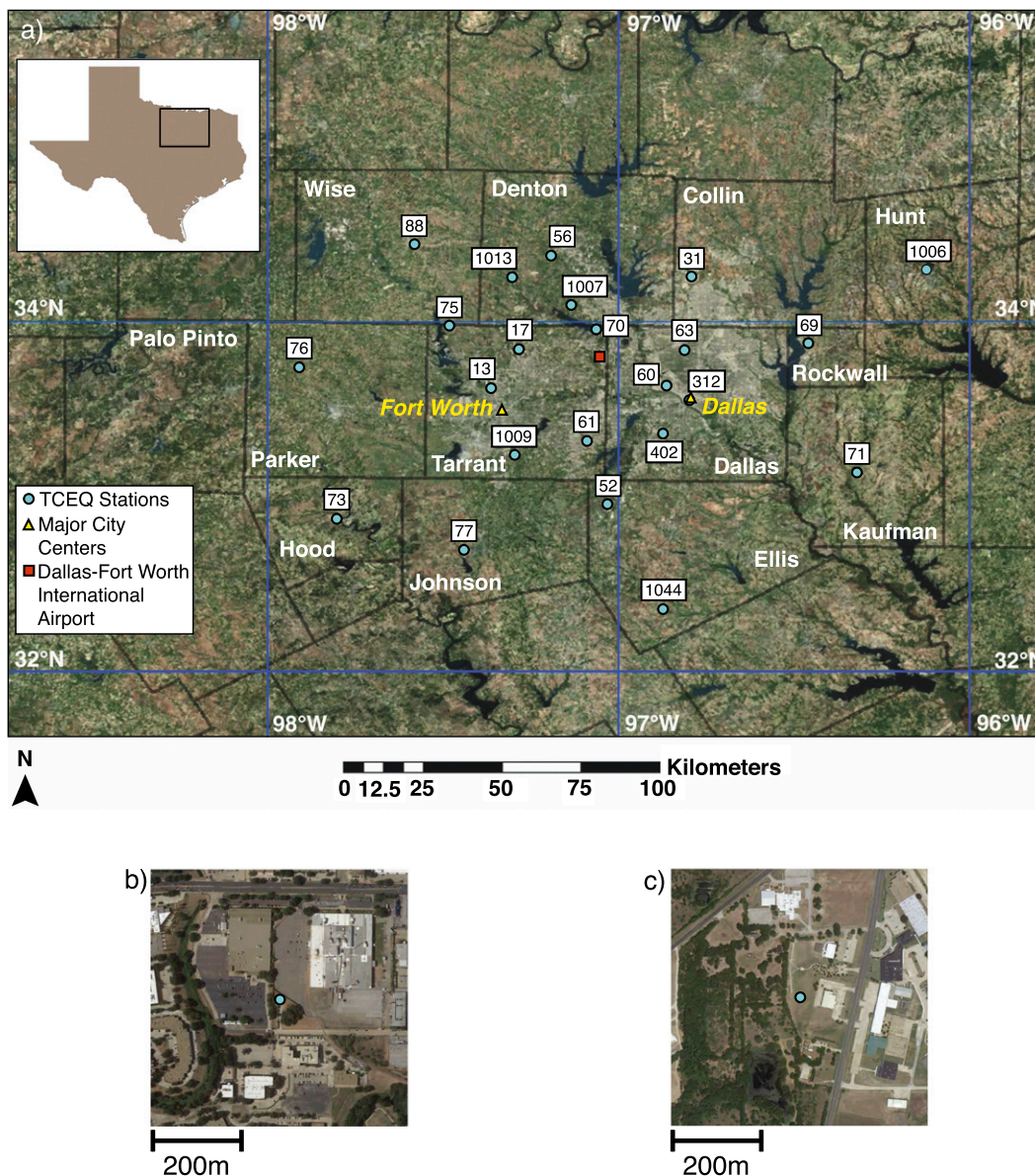E-mail: awinguth@uta.edu

FIG. 1. (a) Environmental Systems Research Institute, Inc., (esri) ArcGIS software map of north-central Texas including urban centers of Dallas and Fort Worth and TCEQ sites. High-resolution aerial photography from Google Maps of the urban surfaces near the TCEQ sites of (b) Dallas Hinton (CAMS 60) and (c) Kaufman (CAMS 70). ArcGIS, version 10 (available online at http://www.arcgis.com), uses a composite of the following data sources: U.S. Department of Agriculture (USDA); U.S. Geological Survey (USGS); Instituto Geográfico Nacional; Instituto Geográfico Português; GeoEye, Inc.; AeroGRID, Ltd.; AEX Aerials Maps and Data, Inc.; esri; GetMapping, Ltd.; I-CUBE, Inc.; and the GIS user community. The high-resolution map is a composite of data from DigitalGlobe, Inc.; GeoEye; Sanborn Map Company, Inc.; Texas Orthoimagery Program; USGS; and USDA Farm Service Agency.

and wind over an urbanized area can occur if frontal systems, like cold fronts with high cloud cover (Hobbs et al. 1990), or mesofronts associated with thunderstorms pass through the area. In the absence of these frontal systems, cloud cover generally reduces the nocturnal canopy layer UHI linearly (Runnalls and Oke 2000; Christen and Vogt 2004), due to an increase in

incident longwave radiation at night, which can lead to reduced cooling, especially of rural surfaces with a large sky-view factor (Oke 1982).

North-central Texas (Fig. 1a) encompasses 16 counties within an area of $33\,138\,\mathrm{km}^2$ and is the fourth-largest metropolitan area in the United States, which includes the cities of Dallas ($32°46'$N, $96°48'$W) and Fort Worth

TABLE 1. Population density for north-central Texas.

County	Census 2000 population*	Census 2010 population	Population change 2000–10 (%)	Area** (m^2)	Density (persons per km^2), 2000	Density (persons per km^2), 2010	Change in density (%, 2000–10)
Collin	491 675	782 341	59	2294	214.33	341.04	59
Dallas	2 218 899	2 368 139	7	2352	943.27	1006.71	7
Denton	432 976	662 614	53	2469	175.36	268.37	53
Ellis	111 360	149 610	34	2464	45.19	60.71	34
Erath	33 001	37 890	15	2822	11.69	13.42	15
Hood	41 100	51 182	25	1131	36.33	45.25	25
Hunt	76 596	86 129	12	2284	33.54	37.71	12
Johnson	126 811	150 934	19	1902	66.67	79.36	19
Kaufman	71 313	103 350	45	2090	34.12	49.45	45
Navarro	45 124	47 735	6	2813	16.04	16.97	6
Palo Pinto	27 026	28 111	4	2552	10.59	11.02	4
Parker	88 495	116 927	32	2357	37.55	49.62	32
Rockwall	43 080	78 337	82	385	111.81	203.31	82
Somervell	6809	8490	25	497	13.70	17.08	25
Tarrant	1 446 219	1 809 034	25	2336	619.18	774.52	25
Wise	48 793	59 127	21	2389	20.42	24.75	21
Region	5 309 277	6 539 950	23	33 138	160.22	197.36	23

* Census data may be found online (http://www.census.gov/main/www/access.html).
** Areas are obtained from the North Central Texas Council of Government.

(32°45′N, 97°19′W). This metropolitan area lies at the upper margin of the coastal plain, and is located approximately 400 km north of the Gulf of Mexico, with elevations ranging from 120 to 350 m. Over the last several decades, the economic and demographic structure of the north-central Texas region has undergone radical changes. Between 2000 and 2010, it experienced a population density growth of ~23% (Table 1). By 2050 the region is projected to be a "megacity" with ~15 million inhabitants (Vision North Texas 2009). The rapid industrialization and urbanization of the area, particularly the suburban sprawl interlinking major city centers, has resulted in a concentration of socioeconomic growth and land-use changes. This includes a greater density of impervious surfaces, such as highways and streets, parking lots, buildings, and commercial and industrial areas, as well as increased air pollution and energy consumption, and a consistent rise in the canopy layer UHI. The canopy layer UHI is influenced by the local land surface usage and land coverage (Chandler 1961), regional climate variations (Lowry 1977; Winkler et al. 1981), large-scale climate variability (Trenberth and Shea 2005; Seager and Vecchi 2010), and long-term climate change (McCarthy et al. 2010) due to meteorological variables, like cloud cover, wind speed, and soil moisture (Runnalls and Oke 2000).

The Dallas–Fort Worth climate is classified as humid subtropical, with 8 months above 20°C and dry winters (Fig. 2; Köppen–Geiger classification Cfa; Köppen 1936; Peel et al. 2007). The precipitation gradient of

north-central Texas is remarkable, with a difference of about 304 mm yr^{-1} between Palo Pinto County in the west and Rockwall County in the east (Nielsen-Gammon 2011). The largest portion of the annual precipitation results from thunderstorm activity, which occurs most frequently in the spring, and is characterized by occasional heavy rainfall over brief periods of time. Summer
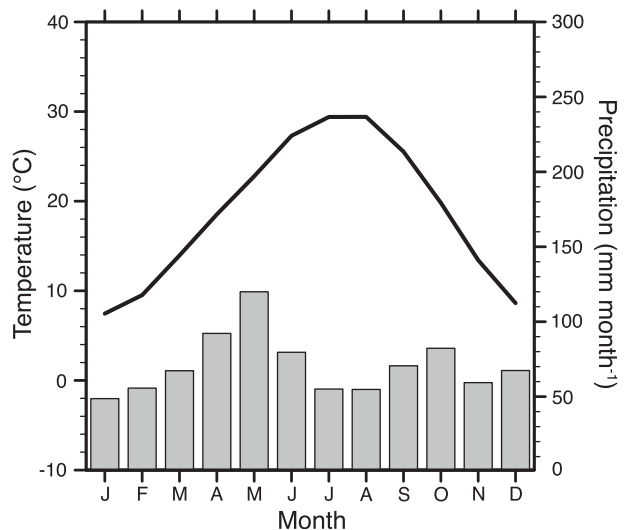

FIG. 2. Monthly mean temperature (solid line) and precipitation (bars) for Dallas–Fort Worth averaged from 1900 to 2011 (Source: NOAA/NWS 2012b). Annual mean temperature is 18.8°C, and annual precipitation is 839.91 mm yr^{-1}.

TABLE 2. List of TCEQ sites used for this study. Altitude is above mean sea level. LCZs of urban landscape are classified following Stewart (2011b): large low-rise (8), sparsely built (9), and bush and shrub (C). Here, OFW refers to Old Fort Worth Road and DISH refers to the town of Dish in Denton County, Texas.

Identifier	Location	Lat	Lon	Alt (m)	LCZ	Activation date
0013	Fort Worth Northwest	32°48′21″	−97°21′24″	198	9*	1 Jan 1975
0017	Keller	32°55′21″	−97°16′56″	232	9	11 Feb 1981
0031	Frisco	33°7′57″	−96°47′11″	232	9	7 May 1992
0052	Midlothian OFW	32°28′55″	−97°1′37″	195	C	7 Nov 1994
0056	Denton Airport South	33°13′9″	−97°11′47″	183	9*	16 Feb 1998
0060	Dallas Hinton	32°49′12″	−96°51′36″	122	8	1 Jan 1986
0061	Arlington Municipal Airport	32°39′23″	−97°5′19″	183	9*	17 Jan 2002
0063	Dallas North No. 2	32°55′9″	−96°48′31″	195	9	2 Nov 1998
0069	Rockwall Heath	32°56′11″	−96°27′33″	165	9	8 Aug 2000
0070	Grapevine Fairway	32°59′3″	−97°3′49″	165	C	4 Aug 2000
0071	Kaufman	32°33′54″	−96°19′4″	128	9	11 Sep 2000
0073	Granbury	32°26′32″	−97°48′13″	226	8	9 May 2000
0075	Eagle Mountain Lake	32°59′16″	−97°28′38″	226	C	6 Jun 2000
0076	Parker County	32°52′8″	−97°54′21″	347	C	26 Jul 2000
0077	Cleburne Airport	32°21′13″	−97°26′12″	195	9*	10 May 2000
0088	Decatur Thompson	33°13′18″	−97°35′4″	317	9	6 Oct 2010
0312	Convention Center	32°46′27″	−96°47′52″	134	8	1 Jan 1979
0402	Dallas Redbird Airport	32°40′35″	−96°52′19″	192	9*	1 Jan 1995
1006	Greenville	33°9′11″	−96°6′56″	165	9	20 Mar 2003
1007	Flower Mound Shiloh	33°2′45″	−97°7′48″	195	9	27 Oct 2010
1009	Everman Johnson Park	32°37′16″	−97°17′25″	195	9	28 Jun 2011
1013	DISH Airfield	33°7′51″	−97°17′52″	213	9*	31 Mar 2010
1032	Pilot Point	33°24′38″	−96°56′41″	201	9	4 Apr 2006
1044	Italy	32°10′32″	−96°52′13″	165	9	21 Aug 2007

* Airport.

temperatures are generally high and were especially so during the severe drought in 2011, when daytime temperatures exceeded 37.8°C (100°F; NOAA/NWS 2012a) for 71 days, the longest heat wave on record for the area.

Several studies have supported the hypothesis that droughts over the Great Plains are linked to cold sea surface temperature (SST) anomalies in the tropical Pacific Ocean (Trenberth et al. 1988; Trenberth and Branstator 1992; Palmer and Brankovic 1989; Ortegren 2008; Seager et al. 2009). The 2010–11 drought in Texas was likely amplified by strong La Niña conditions, together with a positive phase of the Atlantic multidecadal oscillation (McCabe et al. 2004; Mo et al. 2009; Nielsen-Gammon 2012). Low rural soil moisture during the previous winter, also noted as a factor during the 2003 heat wave in Paris, France (Cassou et al. 2005; Dousset et al. 2007), may have enhanced the drought in north-central Texas (Hong and Kalnay 2002). Anthropogenic land-use changes could have further intensified the drought conditions (Cook et al. 2009).

In this paper, the canopy layer UHI of Dallas–Fort Worth (DFW) is investigated by comparing measurements from urban meteorological stations with the rural area stations in the perimeter of the region, as well as by using infrared satellite data. The methodology of this study is similar to the approach used by Oke (1982) and Figuerola and Mazzeo (1998), in which the structure of the heat island is outlined using near-surface temperatures. The influence that climate variability and extremes, especially severe droughts, has on the heat island is examined, with a focus on the maximum heat island for the summer 2011 heat wave.

2. Methods

Two datasets were used for the analysis of the Dallas–Fort Worth heat island: hourly data collected from the Continual Ambient Monitoring Stations (CAMS) implemented by the Texas Commission for Environmental Quality (TCEQ 2012), and daily temperature extremes from the National Weather Service (NWS) Cooperative Observer Program (COOP; NOAA/NESDIS 2012). To assess the spatial properties of the heat island, hourly differences in temperature between 24 TCEQ meteorological stations throughout the metropolitan area (Table 2) are used. The magnitude of the UHI is the temperature difference between the representative urban (Dallas Hinton, CAMS 60) and rural (Kaufman, CAMS 71) stations, which were chosen based on the availability of a long-term record that covered the period of the study, and preliminary analysis of screening temperatures and remotely sensed temperatures of the area.

All TCEQ CAMS sites in the Dallas–Fort Worth area collect temperature, wind speed, and wind direction data using the Climatronics Corporation F460 Utility Wind System. The Dallas Hinton site (CAMS 60) and the Dallas Executive Airport site (CAMS 402), operated by the city of Dallas for TCEQ, have been running this system since April 2011 and April 2012, respectively. The temperature, wind speed, and wind direction sensors are located on towers approximately 10 m high, secured to a cross-arm. Their accuracies are as follow: $\pm 0.15°$C for the screening temperature, $\pm 2°$ for wind direction, and $\pm 0.07\,\mathrm{m\,s}^{-1}$ for wind speed, with a threshold of $0.22\,\mathrm{m\,s}^{-1}$.

Although CAMS 312 (Dallas Convention Center) is closer to the downtown urban center than CAMS 60, it is located on the roof of the convention center, with the sensors close to the roof surface. This may have influenced the temperatures recorded at the site, which were consistently lower or the same as those recorded at CAMS 60, which is located about 7 km from, and 310° (NW) of downtown Dallas. Measurements obtained at CAMS 60 are influenced by nearby trees, a parking lot, a creek bed (180 m away), and commercial buildings (60 m away). There are large, one- to three-story low buildings separated by extensive surfaces in the vicinity of this station, which are classified as local climate zone (LCZ) 8, with a sky-view factor of >0.7 (Stewart 2011b; Fig. 1b). This station is also located 200 m from a four-lane divided road (Fig. 1b). Kaufman and Italy (CAMS 1044) consistently recorded the lowest temperatures in the area; however, CAMS 1044 was not activated until 2007, so CAMS 71 was chosen as the representative rural station for the 2001–11 period. Data from CAMS 71 are potentially influenced by a nearby development to the east and the town of Kaufman to the north, as well as a pond 200 m south of the station (Fig. 1c). Adjacent to the Kaufman site (CAMS 71) is sparsely built landscape, surrounded by small- to medium-size buildings to the west, east, and north, classified as LCZ 9 with a sky-view factor of >0.8.

The difference in altitude between CAMS 60 and CAMS 71 is negligible (~6 m; Table 2). However, there are significant topographic differences between the Parker County site (CAMS 76) and the Kaufman site (CAMS 71) that could result in a topographic-induced temperature difference of up to 2.7°C if a radiosonde lapse rate of 12.5°C km^{-1} for the lower troposphere in July 2011 is assumed. This lapse rate was computed from the mean temperature profile for the NWS Fort Worth site, obtained from the National Climatic Data Center's (NCDC) integrated global radiosonde archive (NOAA/NCDC 2012).

The nighttime canopy UHIs are linked to contrasts in soil moisture, evapotranspiration, increased absorption of thermal radiation and reemission by a polluted atmosphere, longwave radiation loss from the ground, and the roughness flow between urban and rural surfaces (Oke 1987). For example, temperature measurements from the Kaufman site (CAMS 71) are significantly influenced by latent heat fluxes of the surrounding natural land cover (Fig. 1b), whereas the Dallas site (CAMS 60) is located in close proximity to parking lots and buildings (Fig. 1c).

As discussed in Oke and Maxwell (1975) and Fortuniak et al. (2006), the heat island will be maximal when the wind speed and humidity are low, and there is clear sky. The temperature differences between CAMS 60 and CAMS 71, representative of the maximum UHI, were calculated for each hour of January and July 2011. The data were separated into two groups based on critical wind speed and precipitation, following the Figuerola and Mazzeo (1998) method. The first class of data consists of low-wind days with resultant wind speeds $\leq 2\,\mathrm{m\,s}^{-1}$ and no precipitation at the time the maximum heat island occurred. The second class consists of windy days with resultant wind speeds $> 2\,\mathrm{m\,s}^{-1}$ and/or some precipitation. Since TCEQ does not record precipitation, the data from the COOP station nearest to CAMS 60 have been used for precipitation (Dallas Love Field Airport; Table 3). To assess the effects of wind, precipitation, and cloud cover on the heat island, three subsets of hourly temperature differences between the urban and rural stations were analyzed daily for January and July 2011: the maximum positive heat islands of "low wind" days, the maximum positive heat islands for windy days, and the maximum negative heat island on days when one occurred. At the time of the maximum heat island, at least scattered cloud cover (1–4 octas) was identified from the COOP observations; however, there was insufficient data coverage available for days with a clear sky (0 octa).

3. Results

a. Diurnal and seasonal variations of the UHI

In this section, the differences in the diurnal and seasonal temperatures between the urban and rural surfaces are examined. Diurnal variations are unimodal, a trait identified for other cities [e.g., Chicago, Illinois (Ackerman 1985); Vancouver, British Columbia, Canada (Oke 1982)], and are stronger than seasonal variations. The three groups of hourly temperature differences between the urban and rural stations classified in section 2 (Fig. 3a) were used to analyze the maximum diurnal heat island. Of the days in January and July 2011, 74% and 52%, respectively, met low-wind criteria (Table 4; Fig. 3a) and were used to

TABLE 3. List of NWS/COOP sites used for this study. Altitude is above mean sea level. For LSZ classification see Table 2 and the text.

Identifier	Location	Lat	Lon	Elev (m)	LCZ	Activation date
410518	Bardwell Dam	32°15′47″	−96°38′13″	141	9	4 Jan 2000
411063	Bridgeport	33°12′21″	−97°46′34″	234	9	1 Sep 2007
411246	Burleson	32°30′24″	−97°20′39″	232	8	5 Jun 2006
412242	DFW International Airport	32°53′52″	−97°1′8″	171	8	14 Aug 1974
412244	Dallas Love Field	32°51′7″	−96°51′20″	134	8	1 Aug 1939
412334	Decatur	33°16′24″	−97°34′37″	298	9	29 Jun 2001
412404	Denton 2 Southeast	33°11′57″	−97°6′18″	192	8	1 Feb 2009
413133	Ferris	33°7′51″	−97°17′52″	143	9	7 Jan 2009
413284	Fort Worth Meacham Field	32°49′9″	−97°21′41″	209	8	1 Jan 1998
413289	Fort Worth Nature Center	32°50′50″	−97°28′34″	188	9	22 Nov 2002
413285	Fort Worth NWS Forecast Office	32°50′2″	−97°17′51″	196	8	1 Jun 2003
413675	Granbury	32°26′32″	−97°48′13″	237	8	2 Feb 2004
413691	Grapevine Dam	32°57′2″	−97°3′19″	178	8	1 Jan 2000
414597	Joe Pool Lake	32°38′26″	−96°58′29″	180	9	1 Jan 2000
415094	Lavon Dam	33°2′7″	−96°29′10″	155	9	1 Jan 2000
415958	Mineral Wells Airport	32°46′54″	−98°3′37″	283	9	1 Jun 1989
419522	Waxahachie	32°25′41″	−96°50′32″	191	8	21 Jan 2006
419532	Weatherford	32°44′54″	−97°46′12″	291	9	19 Oct 2001

calculate the daily maximum UHI. In the summertime (July), the heat island was observed immediately after the monthly mean sunset at 1935 central standard time (CST), and peaked about 1.5 h later at 2100 CST. In the evening, near sunset, relatively rapid cooling at the rural station, in comparison with the urban station, occurs as the surface is exposed to a net energy transfer from the stable and calm layer (Fig. 4), resulting in a maximum heat island. Additional peaks of the heat island are related to differences between urban and rural cooling rates around sunset (Oke 1982).

For the windy days in July, multiple maxima of the heat island occur just after sunset (Fig. 3b), but in winter, high wind speeds, high soil moisture, and increased cloud cover lead to a less pronounced UHI. The duration of the DFW canopy UHI is about the same as that found for Buenos Aires, Argentina (Figuerola and Mazzeo 1998), a city in the same climate zone and located at about the same latitude; however, peak temperature differences occur about 1 h earlier. This is potentially related to the differences in urban and rural landscapes between the cities, and also to the temperature advection from the Rio de La Plata that influences the UHI of Buenos Aires (Figuerola and Mazzeo 1998). The maximum negative heat island in July (Fig. 3c) typically occurs during the day between 0700 and 1600 CST, with a peak at 1100 CST, about 5.5 h after sunrise. The negative heat island is likely related to the slower warm-up of urban surfaces (Oke 1987). The winter peak occurs at 0900 CST, about 2 h earlier than the summer peak.

Other important influences on the diurnal UHI cycle include the greater daytime sensible heat storage of urban areas, due to the thermal conductivity of building

and construction materials. Man-made surfaces and constructions also cause turbulent heat transport, further amplifying the heat island [see Oke (1987) and Arnfield (2003) for a review]. The large storage of heat by urban surfaces during the day and subsequent release at night (Oke et al. 1999) is sufficient to support weak convective sensible heat, whereas evaporative fluxes, particularly during years of drought, remain small. In downtown Dallas (CAMS 60), buildings release anthropogenic heat from their sides, from air conditioning, particularly during heat waves, and from electricity consumption (Sailor and Lu 2004). This anthropogenic heat flux is potentially enhanced by dense traffic, especially during rush hours [∼(0600–1000) and ∼(1500–1900) CST in winter and ∼(0500–0900) and ∼(1400–1800) CST in summer].

To compare the canopy UHI over the course of the year, the time scale for all observations is normalized using the method of Runnalls and Oke (2000). The 24-h day is transformed into a scale from 0 to 2, with 0.5 and 1.5 representing the times of sunset and sunrise, respectively (Fig. 5). Mean monthly sunrise and sunset for Dallas are computed from daily values available from the U.S. Naval Observatory (2012). The values 0 and 1 on the x axis in Fig. 5 represent the midpoints between sunset and sunrise ("midday" and "midnight," respectively). The maximal UHI (5.4°C) occurred at 2000 CST 15 July 2011, whereas the maximal monthly mean value reached 3.4°C in July 2011 at 2100 CST (Fig. 5). This daily extreme UHI estimate is 0.8°C higher than the winter maximum UHI of Buenos Aires. The dissimilarity with Buenos Aires is probably due to differences in heating and cooling rates linked to differences in soil moisture, cloud cover, local
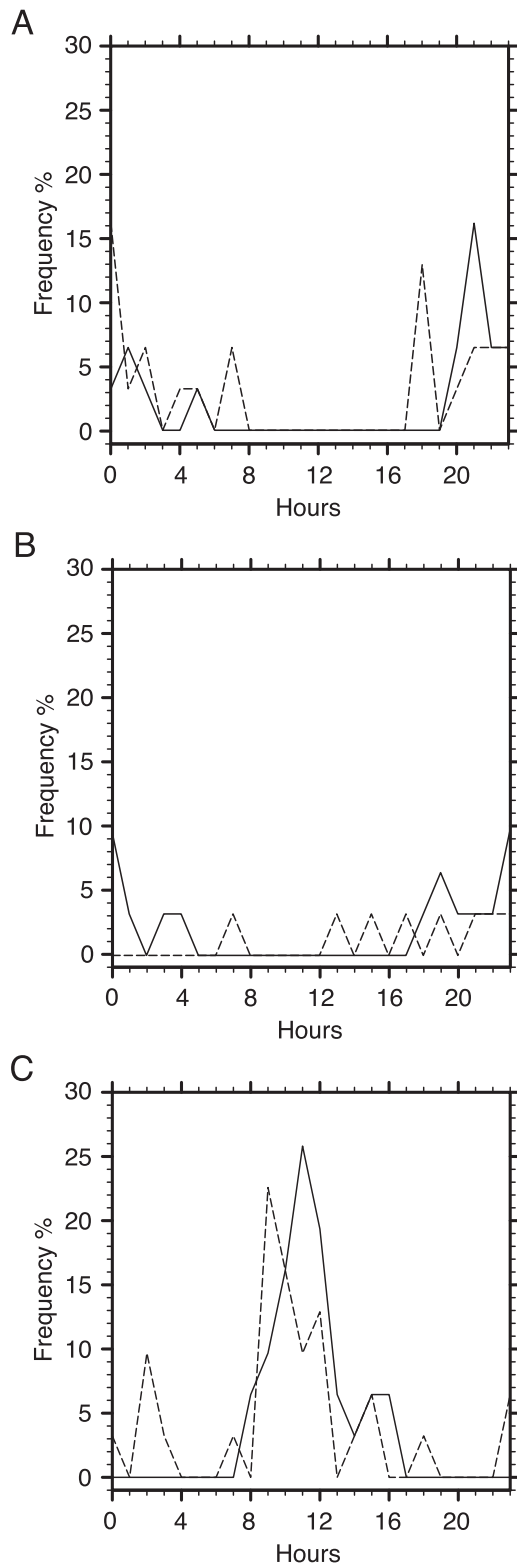
TABLE 4. The number of days during 2011 with low wind ($\leq 2\,m\,s^{-1}$) and windy days ($>2\,m\,s^{-1}$), and the number of days with at least 1 h of negative UHI.

	Low-wind days	Windy days	Days with at least 1 h of negative UHI
Jul	16	15	31
Jan	23	8	25
Total	39	23	56

climate zones (Stewart 2011b), and the proximity of the downtown and rural sites to the city center, as well as anthropogenic developments influencing the rural stations.

Seasonal changes in the heat island are influenced by seasonal synoptic differences, such as increased cloud cover and higher winds during the winter, more precipitation in the spring and fall (Fig. 2; Arnfield 2003), changes in insolation, and general climate variability. The solar elevation angle is low during the winter months, altering the diurnal timing and lowering the intensity of the heat island, while the higher radiation in summer produces a stronger heat island. During January 2011, the soil moisture content was about average at $\sim 550\,kg\,m^{-2}$ (NOAA/OAR/ESRL/PSD 2012b), due to frequent precipitation associated with frontal systems. However, in the summer of 2011, a persistent period of clear skies led to higher-than-normal incoming solar radiation, resulting in low soil moisture content and drought conditions, which increased the cooling rate and, therefore, the UHI.

The seasonal variations of the Dallas–Fort Worth UHI are characterized by a pronounced unimodal feature, which has an amplitude of 0.5°C, in contrast to cities

FIG. 3. Diurnal variation of the relative frequency (percent) of the maximal canopy UHI during July 2011 (solid line) and January (dashed line). (a) Low-wind days with wind speed $\leq 2\,m\,s^{-1}$ and no precipitation, (b) windy days with wind speed $> 2\,m\,s^{-1}$ and/or precipitation, and (c) maximum negative UHI for days on which they occurred. Local time is given in CST.
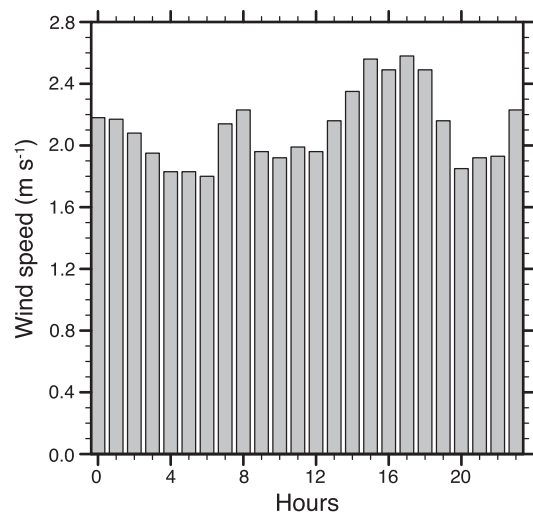
FIG. 4. Diurnal variation in wind speed in downtown Dallas (CAMS 60) during July 2011. Time is given in CST.
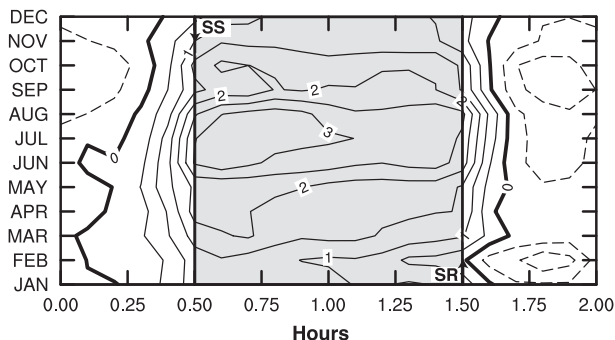
FIG. 5. Normalized diurnal variation of the UHI magnitude over the months/seasons computed from differences (°C) between the temperatures at the Dallas Hinton urban station (CAMS 60) and the Kaufman rural station (CAMS 71) during 2011. Daily time is centered on nighttime and the day length is scaled to 2 [nighttime is gray shaded between mean sunset (SS) and sunrise (SR) each month; see text].

with significant advection of air masses from a nearby river or ocean, which are characterized by a bimodal pattern. Examples of such cities are the Buenos Aires metropolitan area (Figuerola and Mazzeo 1998), which has the same subtropical Köppen–Geiger classification (Cfa) as north-central Texas, and Singapore (Chow and Roth 2006), which is classified as a tropical rain forest climate (Köppen–Geiger classification Af). However, deviations from the unimodal seasonal fluctuation in Dallas–Fort Worth exist because of meteorological changes throughout the year (Fig. 2). A more distinct seasonal fluctuation of the UHI occurs during the evening at 2000 CST with a maximum amplitude of ~1.2°C.

b. Impact of climate variability on interannual fluctuations of the UHI

The annual temperature anomaly of north-central Texas with respect to the 1900–2011 average, shown in Fig. 6, reflects the long-term warming trend of 0.05°C decade^{-1}. The station that recorded these data (COOP 412242) has moved several times, and the locations are as follow: from 1900 to 1939 it was in downtown Fort Worth, from 1940 to 1953 it was at Fort Worth Meacham Field, from 1953 to 1974 it was at the Greater Southwest International Airport, and from 1974 to present it has been at the Dallas–Fort Worth International Airport. The overall warming amounts to 0.58°C over this period, with an even larger increase of 0.14°C from 2001 to 2011. The seasonal trends are particularly strong during the last decade, with an increase in temperature of 0.34°C during summer months and 0.06°C during winter months over this time period (Fig. 6).

Interannual-to-decadal oscillations, such as the Atlantic multidecadal oscillation (AMO; NOAA/OAR/ESRL/PSD 2012a; Bjerknes 1964; Folland et al. 1984; Schlesinger and Ramankutty 1994), El Niño–Southern Oscillation (Bjerknes 1969; Walker 1928), and the Pacific decadal oscillation (Trenberth and Hurrell 1994), influence the climate fluctuations over north-central Texas (Figs. 6 and 7; Diaz and Markgraf 2000). The direct correlation between the AMO index (Enfield et al. 2001) and the DFW air temperature anomaly is substantial ($r = 0.74$). The El Niño signal appears to be anticorrelated with extreme temperatures over this region during the spring (Wolter et al. 1999;
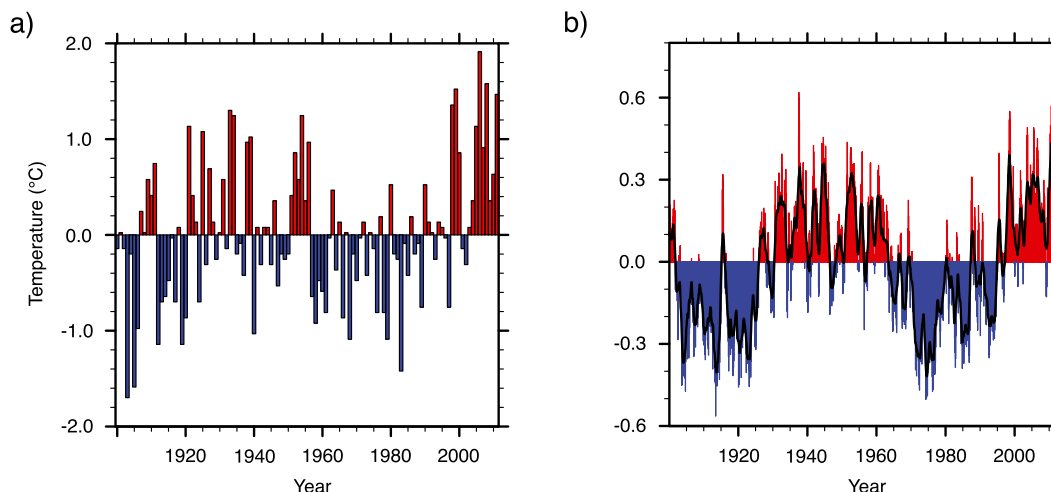

FIG. 6. (a) Annual average surface temperature anomalies (°C) as compared with the average between 1900 and 2011. The data are from NWS/COOP station 412242 (available online at http://www.srh.noaa.gov/fwd/?n=dmotemp). (b) Time series of the AMO index for the same period (colored bars) and smoothed AMO index with a 121-month smoother (black line) (available online at http://www.cdc.noaa.gov/Correlation/amon.us.long.data).
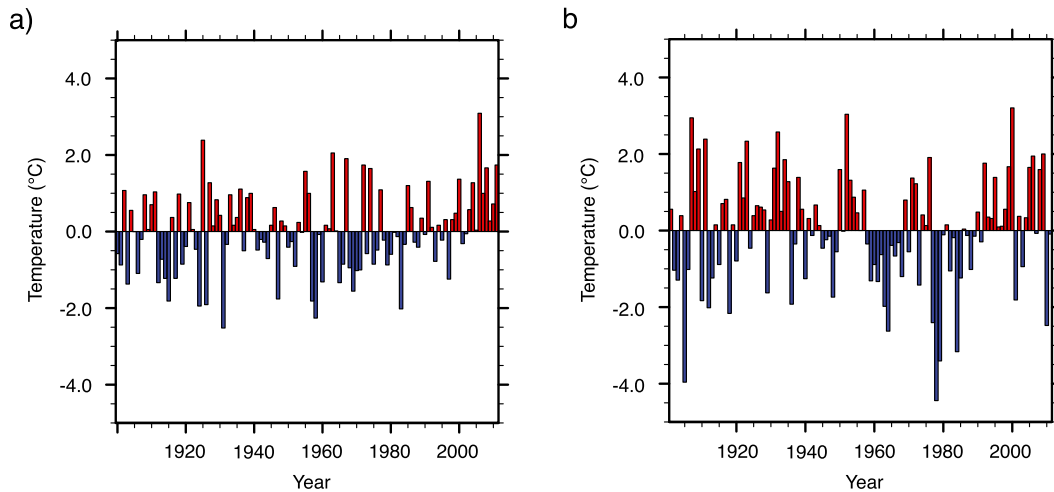
FIG. 7. Summer and winter average surface temperature anomalies (°C) as compared with the average between 1900 and 2011 from NWS/COOP station 412242, used in Fig. 6 for the (a) summer season (June–August) and (b) winter season (December–February).

Nielson-Gammon 2012). The southern plains region tends to experience wetter winters associated with El Niño conditions and drier winters with La Niña conditions.

Climatic variability, especially soil moisture variations and differences in net downward shortwave radiation and in net longwave radiation at the surface due to cloud cover (Runnalls and Oke 2000), as well as the development of urban areas in north-central Texas, have led to significant year-to-year fluctuations in the UHI (Fig. 8). These are characterized by changes in the magnitude of the maximum positive heat island 1–3 h after sunset, and the maximum negative heat island just before noon. The maximum heat island appears to be highly correlated with years of low cloud cover during July, and an associated positive anomaly of excess incoming shortwave radiation flux at the surface of $\sim$20 W m^{-2}. This is in comparison with the mean radiation over the 2001–11 period, as inferred from the National Centers for Environmental Prediction North American Regional Reanalysis (NARR; Mesinger et al. 2006; NOAA/OAR/ESRL/PSD 2012b). This simplified picture is also applicable to the negative canopy UHI, which is related to differences in heating rates between the rural and downtown sites under clear and calm conditions. For example, in 2011, when soil moisture was extremely low, the heating rate of urban surfaces in the morning hours was significantly lower than in rural areas. This created a maximum negative heat island, whereas in other years with heavy precipitation and high soil moisture, a lower negative heat island was observed because of a lower heating rate over the rural area. Reduced net longwave radiation at the surface under cloudy conditions (Runnalls and Oke 2000), as well as enhanced upward moisture flux

in urban areas, diminish the differences in the heating rate over the rural area.

Figure 9 illustrates the correlation between the Palmer drought severity index (PDSI) and the maximum UHI. The calculated Pearson's linear correlation coefficient r is -0.734 and the ρ value is 0.01; that is, there is a significant correlation between the drought and maximum heat island. Two remarkable droughts with different characteristics occurred between 2001 and 2011: the 2005–06 drought (Dong et al. 2011) and the 2010–11 severe drought (Nielsen-Gammon 2012). The 2005–06 drought was persistent, becoming more intense in November 2005 (Dong et al. 2011), whereas drought conditions were more moderate in the winter from 2010 to 2011. In July 2006, drought conditions remained
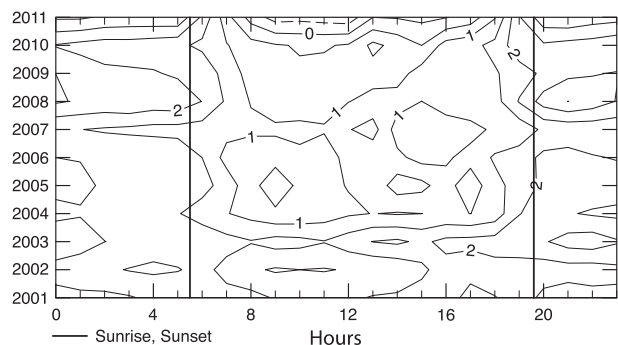

FIG. 8. Isothermals of the average hourly differences (°C) during July between the temperatures at CAMS 60 and CAMS 71 as a function of year and time (in CST). Mean sunrise (0531 CST) and mean sunset (1935 CST) for July are displayed as solid lines. Maximum is observed during July 2011 at 3.4°C. The mean UHI temperature from 2001 to 2011 at 0900 CST is 2.4°C.
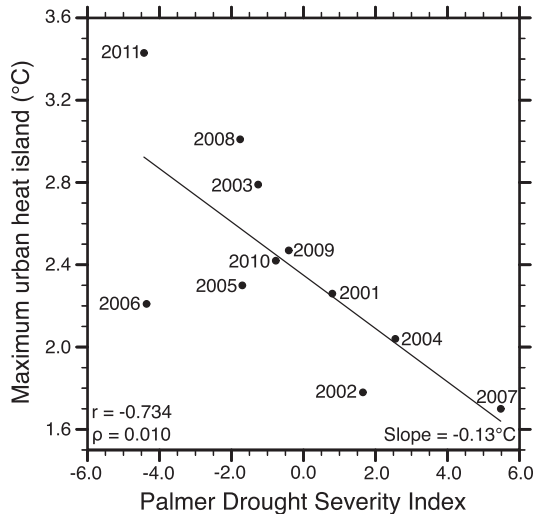
FIG. 9. Correlation between the PDSI and the maximum UHI with an r value of -0.734 and a ρ value of 0.01 for north-central Texas July between 2001 and 2011. Note that a negative PDSI denotes drought conditions; e.g., -2 is moderate drought, -3 is severe drought, and -4 is extreme drought. The UHI is computed between CAMS 60 and CAMS 71.

strong, with lower-than-normal precipitation (8.3 mm) relative to the 1900–2011 mean of 55.1 mm (Fig. 2). July 2011 was characterized by extremely high temperatures, coupled with exceptionally low precipitation (2.3 mm) throughout the summer, which led to a rapid development of a severe drought affecting most of the state of Texas. Even relative to July 2006, soil moisture content in July 2011, inferred from NARR data, was extremely low, and cooling by evapotranspiration was remarkably reduced, thus amplifying the increase in surface temperatures. This led to an extreme heat island during July 2011.

Relative to July 2006, average temperatures in July 2011 at 1600 CST were 3.3°C warmer in Dallas (CAMS 60) and 4.1°C warmer in Kaufman (CAMS 71). Average evening cooling rates from 1600 to 2000 CST in Dallas appeared to be similar in 2006 and 2011 (-0.80°C h^{-1} in 2006 and -0.83°C h^{-1} in 2011), whereas the -1.10°C h^{-1} cooling rate in Kaufman during 2006 was significantly lower than the -1.67°C h^{-1} rate in 2012. The 1.22°C differences between the 2006 and 2011 UHI may be linked to the lower soil moisture content in July 2011 (NOAA/OAR/ESRL/PSD 2012b), and the extreme temperatures at 1600 CST, which reached a maximum value of 38.5°C. The lower water content of the soils would have reduced the heat capacity of the ground and led to higher cooling rates during the evening. In contrast to the years of drought discussed above, a lower-than-normal maximum heat island of 1.64°C occurred in 2007, a year of higher cloud cover and significant rainfall (Dong et al. 2011).

To find an analog to drought conditions in this study, we analyze the maximum UHI under extremely dry seasonal conditions in Mexico City, Mexico, which is located in a subtropical highland climate zone (Köppen–Geiger climate classification Cwb) and typically has very dry winters, with an average precipitation of 11.0 mm in January. Interestingly, the maximum UHI in Mexico City for a dry, 7-day observation period in December 1993, 3.5°C (Oke et al. 1999), appeared in the morning, whereas the July maximum UHI in the Dallas–Fort Worth metropolitan area occurred in the late evening. These differences in the timing and magnitude of the maximum UHI are related to variations in heating and cooling rates between the cities, likely influenced by the local sky-view angle and climate zone, as well as differences in the regional climate and topographic features.

The negative canopy UHI in Dallas, which is not observed in Mexico City, is likely linked to the factors listed above, as well as dissimilarities in the heat storage capacity and associated heating rates between the urban and rural sites under clear and calm conditions, particularly during years of severe drought. For example, in Dallas during 2011, when incoming shortwave radiation was anomalously high and soil moisture was extremely low, the heating rate of urban surfaces in the morning hours was significantly lower than in rural areas. This created a maximum negative heat island, whereas in other years with heavy precipitation and high soil moisture, a significantly smaller negative heat island was observed. This was due to reduced net longwave radiation at the surface, which occurs under cloudy conditions (Runnalls and Oke 2000), as well as enhanced upward moisture flux in the urban areas, which diminished the differences in the heating rate over the rural area.

c. Spatial distribution of the heat island

In this section, the spatial distribution of the heat island during its peak time in July is discussed, with a focus on its exact form and size. Figure 10 shows the characteristic gradual change from lower temperatures in the countryside to higher temperatures in the urbanized areas. The temperature in July 2011 at 2100 CST increases from the rural to the urban area with a horizontal gradient of 0.06°C km^{-1}, which results in ~3.4°C total change between Kaufman (CAMS 71) and downtown Dallas (CAMS 60). A plateau with a temperature change of <0.5°C exists for most of the developed suburban areas in Tarrant and Dallas Counties, particularly north of Dallas and Fort Worth, with peaks of the UHI located near the center of the two major cities. Light southerly to southeasterly winds of about 2.1 m s^{-1} (Fig. 4) advect the warm temperatures toward the northwest, leading to a slight northwest shift of the metropolitan heat island.
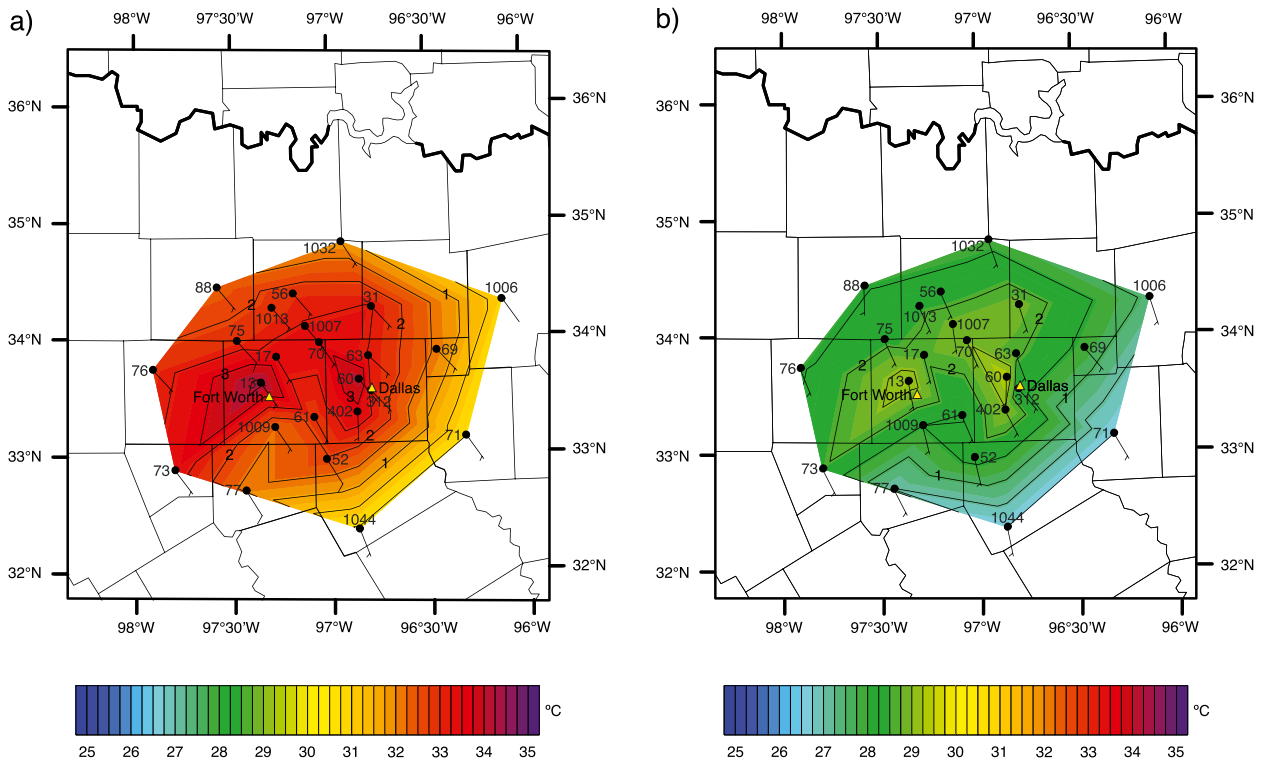
FIG. 10. Maps of the average air temperatures (°C) at screen level at (a) 2100 and (b) 0300 CST in north-central Texas during July 2011, reported by TCEQ stations listed in Table 2. Wind barbs are in knots (1 kt = 0.51 m s^{-1}). Each short barb represents 5 kt, and each long barb is 10 kt. Contour lines show the magnitude of the UHI relative to CAMS 71. Contour line interval is 0.5°C.

Cooling in the southern part of the metroplex is caused by cold-air advection from larger lakes (e.g., Joe Pool Lake), similar to the cooling by advection of air masses from water bodies that has been observed in Chicago (Changnon et al. 1996; Keeler and Kristovich 2012); Kuwait City, Kuwait (Nasrallah et al. 1990); Vancouver (Runnalls and Oke 2000); and Singapore (Chow and Roth 2006).

The impact of urban land surface usage on the heat island is documented by remote sensing data from the Moderate Resolution Imaging Spectroradiometer (MODIS) on board the *Terra* satellite (Fig. 11). Land cover data of vegetation types from the International Biosphere Geosphere Program (IGBP; http://www.igbp.net/; Fig. 11a), coupled with nighttime skin surface temperature data (Fig. 11b), illustrate that developed areas with a high building density further exaggerate the heat island. Note that the mean of the remotely sensed skin surface temperature (Fig. 11b) represents nighttime composites for 8-day intervals and, thus, appears to be cooler than the mean July temperature for 2100 CST (Fig. 10a). However, the remotely sensed skin surface temperature estimate of the maximum UHI of ~3.7°C for downtown Dallas and Fort Worth (Fig. 11b) is about 0.3° higher than air temperature at screening level from the CAMS 60 and CAMS 71 sites, displayed in Fig. 9. Figures 10b

and 12 support the distribution of the heat island with two independent datasets. Note that for Fig. 12, minimum temperatures are used from the NWS/COOP dataset, since they are more representative of nighttime temperatures.

4. Discussion

In this study, the dynamic processes associated with the temporal and spatial distributions, as well as the intensity of the UHI, have been surveyed for a humid subtropical city, and compared with reviews of cities in various climate zones by Oke (1982), Arnfield (2003), and Roth (2007). The general principal limitations of the analysis of the UHI when comparing different cities have been outlined in several studies, for example by Lowry (1977), Oke (1973), and Arnfield (2003), and include differences in climate variability (Winkler et al. 1981) and global climate zones (e.g., Runnalls and Oke 2000; Oke et al. 1991). Use of local climate zones (Stewart 2011b) can provide a method of improved the comparison between cities, since this methodology considers building morphology, construction materials, and anthropogenic-induced heat fluxes, as well as vegetation cover.
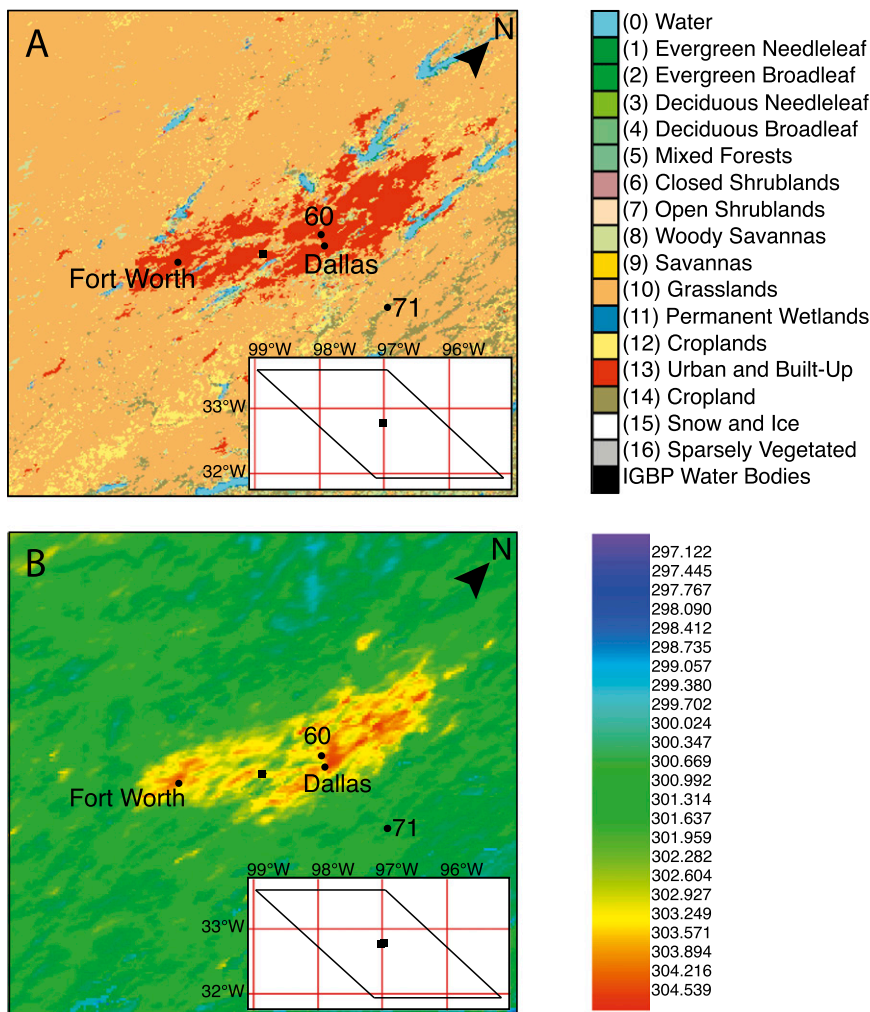
FIG. 11. (a) Remotely sensed land cover of north-central Texas from MODIS land cover classification collection 5 IGBP type 1 2005 (on global 500-m sinusoidal (SIN) grid for 8 days: 28 Jul–4 Aug 2011). (b) Remotely sensed composite data for nighttime MODIS/*Terra* land surface temperature/emissivity (LST; 8-day L3 global 1-km SIN grid) for the same period. The area covered is approximately 201 km (201 pixels) wide and 201 km high. (Available online at http://daac.ornl.gov/get_data.shtml.)

While the most extreme atmospheric and surface conditions can lead to maximum heat islands of 12°C in midlatitudes, tropical and subtropical cities generally appear to have a significantly lower maximum heat island effect of 1°–6°C (e.g., Figuerola and Mazzeo 1998; Streutker 2003; Chen et al. 2003; Roth 2007; Chow and Roth 2006; Brazel et al. 2000; Goldreich 1992), as supported by this study. Nocturnal instantaneous UHI maxima can exceed this estimate by up to 2°C, for example in Mexico City (Jauregui 1993, 1997), as a result of a period of extremely low relative humidity during winter. This is the result of a combination of factors, like rural to urban differences in local heat storage and associated sky-view factor, soil moisture, and other parameters that influence the surface energy balance. In contrast, cities in humid subtropical climates with a Köppen–Geiger classification of Cfa, such as Atlanta, Georgia (monthly mean maximum UHI of 3.4°C; Dixon and Mote 2003); Shanghai, China (instantaneous maximum UHI 5°C and mean maximum UHI of 1.1°C; Jusuf et al. 2007); Buenos Aires (monthly mean maximum UHI 4.6°C; Figuerola and Mazzeo 1998); Houston, Texas (mean maximum 3.19 ±0.08°C; Streutker 2003); and the Dallas–Fort Worth metropolitan area (instantaneous maximum UHI of 5.4°C; monthly mean maximum UHI of 3.4°C and July mean of 2.40 ±0.52°C for 2001–11, as derived from this study) generally have a lower nocturnal maximal UHI, possibly because of limited evaporation due
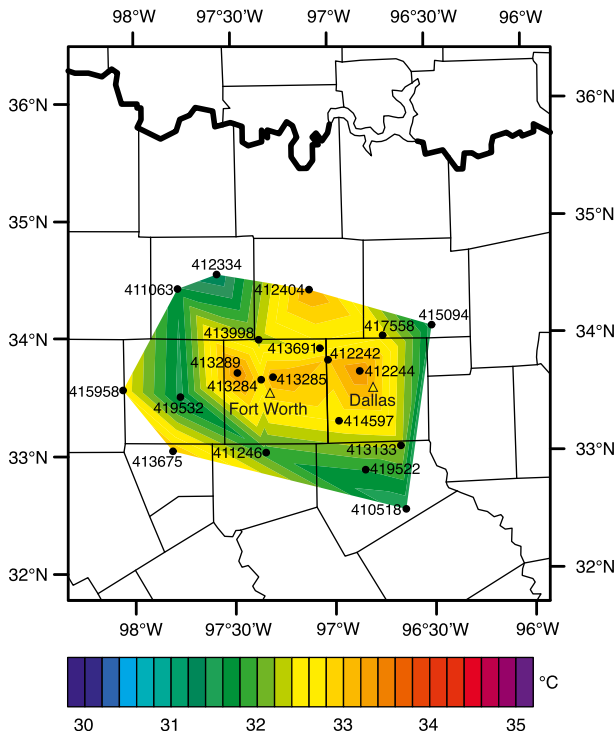
FIG. 12. Map of average minimum temperatures in north-central Texas for July 2011, as computed from NWS/COOP stations listed in Table 3.

at screening level for Dallas (CAMS 60) are up to 0.3°C for July 2011, which may be partially related to the thermodynamic properties of the surface, including upward and downward thermal radiation, latent heat and sensible heat fluxes, as well as heat transport by advective and turbulent processes (Voogt and Oke 2003). The remotely sensed surface skin estimate of the maximum nocturnal UHI of the Dallas–Fort Worth metropolitan area of ~3.7°C is about 0.5°C higher than that of Houston (3.19° ± 0.08°C from July 1999 to June 2001), which is in the proximity of the Gulf of Mexico. The difference in the skin temperature–based nocturnal maximum UHIs between the two cities is of a complex nature, and is partially linked to differences in the standard deviation and sampling size, as well as the difference in the time frame that was studied.

In the Dallas–Fort Worth metropolitan area, the difference between the sky-view factor of the downtown sites and the rural stations, which are increasingly affected by urban sprawl, is relatively small because of a low building density in most of the urban areas. The Dallas Hinton site CAMS 60 is located in close proximity to the downtown area (as discussed in section 2), in a relatively open space with only low building structures. This higher sky-view factor, when compared to urban stations in cities that are more densely built, reduces the average heat island.

The increase of the north-central Texas heat island by 0.08°C over the observed period from 2001 to 2011 is comparable to the long-term warming trend (Fig. 6). Note that the largest amount of urbanization, associated with a decrease in the sky-view factor and soil moisture content, occurred north of site CAMS 60 (Collin and Denton Counties; Table 1). The development in the city centers remained constant, whereas the total growth of the region was characterized by widespread urban sprawl in the suburbs (Table 1). The impact of rapid urbanization on the spatial extent and magnitude of the canopy layer air temperature heat island has been documented using ground-based stations in Baltimore, Maryland, and Phoenix, Arizona (Brazel et al. 2000; Brazel and Heisler 2009), and remote sensing data from Houston (Streutker 2003). While worldwide anthropogenic land surface changes contribute less than 0.3°C century^{-1} (Kalnay and Cai 2003) to the overall global temperature increase, urbanization heavily impacts the regional climate (Fig. 11; Sagan et al. 1979; Voogt 2003; Rizwan et al. 2008; McCarthy et al. 2010). Similarly, the rapid growth of the Dallas–Fort Worth metropolitan area likely influenced the average temperature increase of 0.58°C in the region over the period of 1900–2011 (Fig. 6).

In the U.S. southwest, future climate projections to 2100 indicate that the temperature and hydrological patterns

to the increased vapor pressure of near-saturated air masses and typically higher soil moisture content in these humid climates.

During severe drought conditions, like those in Texas during 2010 and 2011, the UHI is significantly amplified. In July 2011, the instantaneous nocturnal screening maximum UHI of the Dallas–Fort Worth area increased relative to the July 2001–2011 mean by up to 3.0°C, and was comparable to UHI estimates for cities with extreme seasons, like Mexico City. As discussed in Grimmond and Oke (1999) and Roth (2007), in extremely dry environments, latent heat fluxes are significantly reduced and heat storage density is increased. These factors are influenced by differences in heating rates, particularly after sunset and sunrise, between the rural and urban sites. The maximal UHI also depends on the types and amount of vegetative cover, which deteriorates during drought conditions, at the different meteorological stations. Cities located in biomes with vegetation that is predominantly characterized by grasslands and shrubs, including Dallas–Fort Worth, generally have a lower maximum nocturnal UHI, as supported by a remote sensing study by Imhoff et al. (2010).

Differences between the remotely sensed surface skin temperature, estimated by the MODIS on the *Terra* satellite (Fig. 11), and the nocturnal canopy air temperature

will undergo significant changes, likely shifting the region to a hotter and drier climate (Seager and Vecchi 2010; Peacock 2012), which could accelerate the anthropogenic heat release in metropolitan areas (McCarthy et al. 2010). Future climate scenarios with intermediate prospective greenhouse gas emissions (Special Report on Emissions Scenarios scenario A1B; Solomon et al. 2007) predict that the mean temperature over the Dallas–Fort Worth area will increase ~2.2°C by 2050 (Nielsen-Gammon 2011). This temperature rise could be exacerbated in urban areas, like Dallas–Fort Worth, during times of extreme drought, which will likely be amplified by an increase in the frequency of extreme heat waves.

5. Conclusions

This study characterizes the canopy heat island of a large metropolitan area with a humid, subtropical climate using data from a recently installed air quality network. The maximum temperature differences between urban and rural stations occurred after sunset, and reached a peak of 3.4°C in July 2011, during a particularly severe heat wave and drought. This drought also produced a "cool" island observed during morning hours after sunrise in response to a slower warming of urban surfaces. In contrast, high soil moisture and cloud cover have a damping effect on the heat island.

Remote sensing images support the ground-based measurements, and emphasize the correlation between the heat island and urban surface coverage. Since Dallas–Fort Worth is the fourth-largest metroplex in the United States, its heat island covers a significant area and influences the regional climate. It would be of future interest, and certainly a challenge, to simulate the urban boundary layer and downwind urban plume with a highly resolving climate model (e.g., Lemonsu et al. 2009; Bohnenstengel et al. 2011). The model simulation, together with detailed satellite imagery, could be used to analyze heat fluxes and causes of the region's heat island (Miao et al. 2009). Such a study may also contribute to the improvement of small-scale processes in global climate models used for future climate prediction, and improve air quality prediction for urbanized areas (e.g., Prather et al. 2003; Hogrefe et al. 2004; Mickley et al. 2004; Leung and Gustafson 2005; Murazaki and Hess 2006; Racherla and Adams 2006; Tao et al. 2007; Jiang et al. 2008). Mitigation of the UHI is necessary to reduce the associated health-related (Braga et al. 2002) and energy-related costs (Rizwan et al. 2008; Gaffin et al. 2012), and to avoid a future amplification of the problems associated with urban-induced climate change.

REFERENCES

Ackerman, B., 1985: Temporal march of the Chicago heat island. *J. Climate Appl. Meteor.,* **24,** 547–554.

Arnfield, A. J., 2003: Two decades of urban climate research: A review of turbulence, exchanges of energy and water, and the urban heat island. *Int. J. Climatol.,* **23,** 1–26.

Bjerknes, J., 1964: Atlantic air–sea interaction. *Advances in Geophysics,* Vol. 10, Academic Press, 1-82.

——, 1969: Atmospheric teleconnections from the equatorial Pacific. *Mon. Wea. Rev.,* **97,** 163–172.

Bohnenstengel, S. I., S. Evans, P. A. Clark, and S. E. Belcher, 2011: Simulations of the London urban heat island. *Quart. J. Roy. Meteor. Soc.,* **137,** 1625–1640, doi:10.1002/qj.855.

Braga, A. L. F., A. Zanobetti, and J. Schwartz, 2002: The effect of weather on respiratory and cardiovascular deaths in 12 U.S. cities. *Environ. Health Perspect.,* **110,** 859–863.

Brazel, A. J., and G. M. Heisler, 2009: Climatology at urban long-term ecological research sites: Baltimore Ecosystem Study and Central Arizona-Phoenix. *Geogr. Compass,* **3** (1), 22–44.

——, N. Selover, R. Vose, and G. Heisler, 2000: A tale of two climates—Baltimore and Phoenix urban LTER sites. *Climate Res.,* **15,** 123–135.

Cassou, C., L. Terray, and A. S. Phillips, 2005: Tropical Atlantic influence on European heat waves. *J. Climate,* **18,** 2805–2811.

Chandler, T. J., 1961: The changing form of London's urban heat island. *Geography,* **46,** 295–307.

——, 1965: *The Climate of London.* Hutchinson, 292 pp.

Changnon, S. A., K. E. Kunkel, and B. C. Reinke, 1996: Impacts and responses to the 1995 heat wave: A call to action. *Bull. Amer. Meteor. Soc.,* **77,** 1497–1506.

Chen, L., W. Zhu, X. Zhou, and Z. Zhou, 2003: Characteristics of the heat island effect in Shanghai and its possible mechanism. *Adv. Atmos. Sci.,* **20,** 991–1001.

Chow, W. T. L., and M. Roth, 2006: Temporal dynamics of the urban heat island of Singapore. *Int. J. Climatol.,* **26,** 2243–2260.

Christen, A., and R. Vogt, 2004: Energy and radiation balance of a central European city. *Int. J. Climatol.,* **24,** 1395–1421.

Cook, B. I., R. L. Miller, and R. Seager, 2009: Amplification of the North American "Dust Bowl" drought through human induced land degradation. *Proc. Natl. Acad. Sci. USA,* **106,** 4997–5001, doi:10.1073/pnas.0810200106.

Diaz, H. F., and V. Markgraf, 2000: *El Niño and the Southern Oscillation: Multiscale Variability and Global and Regional Impacts.* Cambridge University Press, 496 pp.

Dixon, P. G., and T. L. Mote, 2003: Patterns and causes of Atlanta's urban heat island–initiated precipitation. *J. Appl. Meteor.,* **42,** 1273–1284.

Dong, X., and Coauthors, 2011: Investigation of the 2006 drought and 2007 flood extremes at the Southern Great Plains through an integrative analysis of observations. *J. Geophys. Res.,* **116,** D03204, doi:10.1029/2010JD014776.

Dousset, B., F. Gourmelon, and E. Mauri, 2007: Application of satellite remote sensing for urban risk analysis: A case study of the 2003 extreme heat wave in Paris. *Urban Remote Sensing Joint Event 2007,* Paris, France, IEEE, doi:10.1109/URS.2007.371849.

Enfield, D. B., A. M. Mestas-Nunez, and P. J. Trimble, 2001: The Atlantic multidecadal oscillation and its relationship to

rainfall and river flows in the continental U.S. *Geophys. Res. Lett.,* **28,** 2077–2080.

Figuerola, P. I., and N. A. Mazzeo, 1998: Urban–rural temperature differences in Buenos Aires. *Int. J. Climatol.,* **18,** 1709–1723.

Folland, C. K., D. E. Parker, and F. E. Kates, 1984: Worldwide temperature fluctuations 1856–1981. *Nature,* **310,** 670–673.

Fortuniak, K., K. Kłysik, and J. Wibig, 2006: Urban–rural contrasts of meteorological parameters in Łódz. *Theor. Appl. Climatol.,* **84,** 91–101.

Gaffin, S. R., and Coauthors, 2012: Bright is the new black—Multi-year performance of high-albedo roofs in an urban climate. *Environ. Res. Lett.,* **7,** 014029, doi:10.1088/1748-9326/7/1/014029.

Goldreich, Y., 1992: Urban climate studies in Johannesburg, a subtropical city located on a ridge—A review. *Atmos. Environ.,* **26B,** 407–420.

Grimmond, C. S. B., and T. R. Oke, 1999: Heat storage in urban areas: Local-scale observations and evaluation of a simple model. *J. Appl. Meteor.,* **38,** 922–940.

Hobbs, P. V., J. D. Locatelli, and J. E. Martin, 1990: Cold fronts aloft and the forecasting of precipitation and severe weather east of the Rocky Mountains. *Wea. Forecasting,* **5,** 613–626.

Hogrefe, C., and Coauthors, 2004: Simulating changes in regional air pollution over the eastern United States due to changes in global and regional climate and emissions. *J. Geophys. Res.,* **109,** D22301, doi:10.1029/2004JD004690.

Hong, S.-Y., and E. Kalnay, 2002: The 1998 Oklahoma–Texas drought: Mechanistic experiments with NCEP global and regional models. *J. Climate,* **15,** 945–963.

Howard, L., 1833: *The Climate of London.* Vols. 1–3. Harvey and Dorton, 1002 pp.

Imhoff, M. L., P. Zhang, R. E. Wolfe, and L. Bounoua, 2010: Remote sensing of the urban heat island effect across biomes in the continental USA. *Remote Sens. Environ.,* **114,** 504–513.

Jauregui, E., 1993: Mexico City's urban heat island revisited (Die Wärmeinsel von Mexico City-ein Rückblick). *Erdkunde,* **47,** 185–195.

——, 1997: Heat island development in Mexico City. *Atmos. Environ.,* **31,** 3821–3831.

Jiang, X. Y., C. Wiedinmyer, F. Chen, Z.-L. Yang, and J. C. F. Lo, 2008: Predicted impacts of climate and land-use change on surface ozone in the Houston, Texas, area. *J. Geophys. Res.,* **113,** D20312, doi:10.1029/2008JD009820.

Jusuf, S. K., N. H. Wong, E. Hagen, R. Anggoro, and Y. Hong, 2007: The influence of land use on the urban heat island in Singapore. *Habitat Int.,* **31,** 232–242.

Kalnay, E., and M. Cai, 2003: Impact of urbanization and land-use change on climate. *Nature,* **423,** 528–531.

Keeler, J. M., and D. A. R. Kristovich, 2012: Observations of urban heat island influence on lake-breeze frontal movement. *J. Appl. Meteor. Climatol.,* **51,** 702–710.

Köppen, W., 1936: Das geographische System der Klimate. *Handbuch der Klimatologie,* Band 1, Teil C, W. Köppen and R. Geiger, Eds., Gebr. Borntraeger, 1–44.

Landsberg, H. E., 1981: *The Urban Climate.* Academic Press, 275 pp.

Lemonsu, A., S. Belair, and J. Mailhot, 2009: The new Canadian urban modelling system: Evaluation for two cases from the Joint Urban 2003 Oklahoma City experiment. *Bound.-Layer Meteor.,* **133,** 47–70.

Leung, L. R., and W. I. Gustafson Jr., 2005: Potential regional climate change and implications to U.S. air quality. *Geophys. Res. Lett.,* **32,** L16711, doi:10.1029/2005GL022911.

Lowry, W. P., 1977: Empirical estimation of urban effects on climate: A problem analysis. *J. Appl. Meteor.,* **16,** 129–135.

McCabe, G. J., M. A. Palecki, and J. L. Betancourt, 2004: Pacific and Atlantic Ocean influences on multidecadal drought frequency in the United States. *Proc. Natl. Acad. Sci. USA,* **101,** 4137–4141.

McCarthy, M. P., M. J. Best, and R. A. Betts, 2010: Climate change in cities due to global warming and urban effects. *Geophys. Res. Lett.,* **37,** L09705, doi:10.1029/2010GL042845.

Mesinger, F., and Coauthors, 2006: North American Regional Reanalysis. *Bull. Amer. Meteor. Soc.,* **87,** 343–360.

Miao, S., S. F. Chen, M. A. Lemone, M. Tewari, Q. Li, and Y. Wang, 2009: An observational and modeling study of characteristics of urban heat island and boundary layer structures in Beijing. *J. Appl. Meteor. Climatol.,* **48,** 484–501.

Mickley, L. J., D. J. Jacob, B. D. Field, and D. Rind, 2004: Effects of future climate change on regional air pollution episodes in the United States. *Geophys. Res. Lett.,* **31,** L24103, doi:10.1029/2004GL021216.

Mo, K. C., J. E. Schemm, and S. H. Yoo, 2009: Influence of ENSO and the Atlantic multidecadal oscillation on drought over the United States. *J. Climate,* **22,** 5962–5982.

Murazaki, K., and P. Hess, 2006: How does climate change contribute to surface ozone change over the United States? *J. Geophys. Res.,* **111,** D05301, doi:10.1029/2005JD005873.

Nasrallah, H. A., A. J. Brazel, and R. C. Balling, 1990: Analysis of the Kuwait City urban heat island. *Int. J. Climatol.,* **10,** 401–405.

Nielsen-Gammon, J. W., 2011: The changing climate of Texas. *The Impact of Global Warming on Texas,* G. R. North, J. Schmandt, and J. Clarkson, Eds., University of Texas Press, 39–86.

——, 2012: The 2011 Texas drought: A briefing packet for the Texas Legislature October 31, 2011. Office of the State Climatologist, College of Geosciences, Texas A&M University, 43 pp. [Available online at http://climatexas.tamu.edu/files/2011_drought.pdf.]

NOAA/NCDC, cited 2012: Integrated global radiosonde archive. Integrated Global Radiosonde Archive. [Available online at http://www.ncdc.noaa.gov/oa/climate/igra/.]

NOAA/NESDIS, cited 2012: NWS Cooperative Observer Program (COOP). [Available online at http://www7.ncdc.noaa.gov/IPS/coop/coop.html.]

NOAA/NWS, cited 2012a: Dallas/Fort Worth—Annual and consecutive 100°days. NWS Weather Forecast Office Dallas/Fort Worth. [Available online http://www.srh.noaa.gov/fwd/?n=danncon10.]

——, cited 2012b: Dallas/Fort Worth—Monthly and annual average temperatures. NWS Weather Forecast Office Dallas/Fort Worth. [Available online at http://www.srh.noaa.gov/fwd/?n=dmotemp.]

NOAA/OAR/ESRL/PSD, cited 2012a: AMO index. [Available online at http://www.esrl.noaa.gov/psd/data/timeseries/AMO/.]

——, cited 2012b: NCEP North American Regional Reanalysis. [Available online at http://www.esrl.noaa.gov/psd/.]

Oke, T. R., 1973: City size and the urban heat island. *Atmos. Environ.,* **7,** 769–779.

——, 1978: The distinction between canopy and boundary layer urban heat islands. *Atmosphere,* **14,** 268–277.

——, 1982: The energetic basis of the urban heat island. *Quart. J. Roy. Meteor. Soc.,* **108,** 1–24.

——, 1987: *Boundary Layer Climates.* 2nd ed. Routledge, 435 pp.

——, and G. B. Maxwell, 1975: Urban heat island dynamics in Montreal and Vancouver. *Atmos. Environ.,* **9,** 191–200.

——, G. T. Johnson, D. G. Steyn, and I. D. Watson, 1991: Simulation of surface urban heat islands under 'ideal' conditions at night. Part 2: Diagnosis of causation. *Bound.-Layer Meteor.,* **56,** 339–358.

——, R. A. Spronken-Smith, E. Jauregui, and C. S. B. Grimmond, 1999: The energy balance of central Mexico City during the dry season. *Atmos. Environ.,* **3,** 3919–3930.

Ortegren, J. T., 2008: Tree-ring based reconstruction of multi-year summer droughts in Piedmont and coastal plain climate divisions of the southeastern U.S., 1690–2006. Ph.D. thesis, University of North Carolina at Greensboro, 112 pp.

Palmer, T. N., and C. Brankovic, 1989: The 1988 United States drought linked to anomalous sea surface temperature. *Nature,* **338,** 54–57.

Peacock, S., 2012: Projected twenty-first-century changes in temperature, precipitation, and snow cover over North America in CCSM4. *J. Climate,* **25,** 4405–4429.

Peel, M. C., B. L. Finlayson, and T. A. McMahon, 2007: Updated world map of the Köppen–Geiger climate classification. *Hydrol. Earth Syst. Sci.,* **11,** 1633–1644.

Prather, M., and Coauthors, 2003: Fresh air in the 21st century? *Geophys. Res. Lett.,* **30,** 1100, doi:10.1029/2002GL016285.

Racherla, P. N., and P. J. Adams, 2006: Sensitivity of global tropospheric ozone and fine particulate matter concentrations to climate change. *J. Geophys. Res.,* **111,** D24103, doi:10.1029/2005JD006939.

Rizwan, A. M., D. Y. C. Leung, and L. Chunho, 2008: A review on the generation, determination and mitigation of urban heat island. *J. Environ. Sci.,* **20,** 120–128.

Roth, M., 2007: Review of urban climate research in (sub)tropical regions. *Int. J. Climatol.,* **27,** 1859–1873, doi:10.1002/joc.1591.

Runnalls, K. E., and T. R. Oke, 2000: Dynamics and controls of the near-surface heat island of Vancouver, British Columbia. *Phys. Geogr.,* **21,** 283–304.

Sagan, C., O. B. Toon, and J. B. Pollack, 1979: Anthropogenic albedo changes and the Earth's climate. *Science,* **206,** 1363–1368.

Sailor, D. A., and L. Lu, 2004: A top–down methodology for developing diurnal and seasonal anthropogenic heating profiles for urban areas. *Atmos. Environ.,* **38,** 2737–2748.

Schlesinger, M. E., and N. Ramankutty, 1994: An oscillation in the global climate system of period 65-70 years. *Nature,* **367,** 723–726.

Seager, R., and G. Vecchi, 2010: Greenhouse warming and the 21st century hydroclimate of southwestern North America. *Proc. Natl. Acad. Sci. USA,* **107,** 21 277–21 282.

——, A. Tzanova, and J. Nakamura, 2009: Drought in the southeastern United States: Causes, variability over the last millennium, and the potential for future hydroclimatic change. *J. Climate,* **22,** 5021–5045.

Solomon, S., D. Qin, M. Manning, Z. Chen, M. Marquis, K. Averyt, M. Tignor, and H. L. Miller Jr., Eds., 2007: *Climate Change 2007: The Physical Science Basis.* Cambridge University Press, 996 pp.

Stewart, I. D., 2011a: A systematic review and scientific critique of methodology in modern urban heat island literature. *Int. J. Climatol.,* **31,** 200–217, doi:10.1002/joc.2141.

——, 2011b: Refining the urban heat island. Ph.D. thesis, University of British Columbia, Vancouver, BC, Canada, 352 pp.

Streutker, D., 2003: Satellite-measured growth of the urban heat island of Houston, Texas. *Remote Sens. Environ.,* **85,** 282–289.

Tao, Z., A. Williams, H.-C. Huang, M. Caughey, and X.-Z. Liang, 2007: Sensitivity of U.S. surface ozone to future emissions and climate changes. *Geophys. Res. Lett.,* **34,** L08811, doi:10.1029/2007GL029455.

TCEQ, cited 2012: TCEQ air and water monitoring stations. Texas Commission for Environmental Quality. [Available online at http://www.tceq.texas.gov/cgi-bin/compliance/monops/daily_summary.pl.]

Trenberth, K. E., and G. W. Branstator, 1992: Issues in establishing causes of the 1988 drought over North America. *J. Climate,* **5,** 159–172.

——, and J. W. Hurrell, 1994: Decadal atmosphere–ocean variations in the Pacific. *Climate Dyn.,* **9,** 303–319.

——, and D. J. Shea, 2005: Relation between precipitation and surface temperature. *Geophys. Res. Lett.,* **32,** L14703, doi:10.1029/2005GL022760.

——, G. W. Branstator, and P. A. Arkin, 1988: Origins of the 1988 North American drought. *Science,* **242,** 1640–1645.

U.S. Naval Observatory, cited 2012: Sun or moon rise/set for one year. Astronomical Applications Dept. [Available online at http://aa.usno.navy.mil/data/docs/RS_OneYear.php.]

Vision North Texas, 2009: North Texas 2050, Vision North Texas: Understanding our options for growth, 2009. [Available online at www.visionnorthtexas.org/main.html.]

Voogt, J. A., 2003: Urban heat island. *Causes and Consequences of Global Environmental Change,* Vol. 3, I. Douglas, Ed., *Encyclopedia of Global Environmental Change,* John Wiley and Sons, 660–666.

——, 2010: Urban climate. *Encyclopedia of Urban Studies,* R. Hutchison, Ed., SAGE Publications, 848–853.

——, and T. R. Oke, 2003: Thermal remote sensing of urban climates. *Remote Sens. Environ.,* **86,** 370–384.

Vukovich, F. M., 1971: Theoretical analysis of the effect of mean wind and stability on a heat island circulation characteristic of an urban complex. *Mon. Wea. Rev.,* **99,** 919–926.

Walker, G. T., 1928: World weather. *Mon. Wea. Rev.,* **56,** 167–170.

Winkler, J. A., R. H. Skaggs, and D. G. Baker, 1981: Effects of temperature adjustments on the Minneapolis–St. Paul urban heat island. *J. Appl. Meteor.,* **20,** 1295–1300.

Wolter, K., R. M. Dole, and C. A. Smith, 1999: Short-term climate extremes over the continental United States and ENSO. Part I: Seasonal temperatures. *J. Climate,* **12,** 3255–3272.

Wong, K. K., and R. A. Dirks, 1978: Mesoscale perturbations on airflow in the urban mixing layer. *J. Appl. Meteor.,* **17,** 677–688.

Zhang, D.-L., Y.-X. Shou, R. R. Dickerson, and F. Chen, 2011: Impact of upstream urbanization on the urban heat island effects along the Washington–Baltimore corridor. *J. Appl. Clim. and Meteor.,* **50,** 2012–2029.